RESEARCH ARTICLE

NEUTRINO ASTROPHYSICS

Observation of high-energy neutrinos from the Galactic plane

IceCube Collaboration*†

The origin of high-energy cosmic rays, atomic nuclei that continuously impact Earth's atmosphere, is unknown. Because of deflection by interstellar magnetic fields, cosmic rays produced within the Milky Way arrive at Earth from random directions. However, cosmic rays interact with matter near their sources and during propagation, which produces high-energy neutrinos. We searched for neutrino emission using machine learning techniques applied to 10 years of data from the IceCube Neutrino Observatory. By comparing diffuse emission models to a background-only hypothesis, we identified neutrino emission from the Galactic plane at the 4.5σ level of significance. The signal is consistent with diffuse emission of neutrinos from the Milky Way but could also arise from a population of unresolved point sources.

The Milky Way emits radiation across the electromagnetic spectrum, from radio waves to gamma rays. Observations at different wavelengths provide insight into the structure of the Galaxy and have identified sources of the highest-energy photons. For gamma rays with energies above 1 GeV, the plane of the Milky Way is the most prominent feature visible on the sky (Fig. 1B). Most of this observed gamma-ray flux consists of photons generated by the decay of neutral pions (π^0), themselves produced by cosmic rays (high-energy charged particles) colliding with the interstellar medium within the Milky Way Galaxy (*1*).

Photons can also be produced from interactions of energetic electrons with interstellar photon fields or be absorbed by ambient interstellar matter, so other messengers are needed to determine the cosmic-ray interactions and acceleration sites in the Galaxy. In addition to neutral pions, cosmic-ray interactions also produce charged pions. Charged pions produce neutrinos when they decay. Unlike photons, neutrinos rarely interact on their way to Earth, so they directly trace the location and energetics of the cosmic-ray interactions.

Because both gamma rays and neutrinos arise from the decay of pions, a diffuse neutrino flux concentrated along the Galactic plane has been predicted (*2*–*5*). The expected tera–electron volt energy neutrino flux is shown in Fig. 1D, calculated from the giga–electron volt gamma-ray observation (*1*). In addition to the predicted diffuse emission, the Milky Way is densely populated with numerous high-energy gamma-ray point sources (also visible in Fig. 1B), several classes of which are potential cosmic-ray accelerators and therefore possible neutrino sources (*6*–*10*). This makes the Galactic plane an expected location of neutrino emission.

Previous searches for this signal by using neutrino detectors (*11*–*14*) have not found a statistically significant signal (*P* values ≥0.02). The development of deep learning techniques in data science has produced tools (*15*–*17*) that can identify a larger number of neutrino interactions in detector data, with improved angular resolution over earlier methods. We applied these deep learning tools to data from the IceCube Neutrino Observatory to search for evidence of neutrino emission from the Galactic plane.

Cascade events in IceCube

The IceCube Neutrino Observatory (*18*), located at the South Pole, is designed to detect high-energy (≳1 TeV) astrophysical neutrinos and identify their sources. The detector construction, which deployed instruments within a cubic kilometer of clear ice, was completed in 2011; 5160 digital optical modules (DOMs) were placed at depths between 1.5 and 2.5 km below the surface of the Antarctic glacial ice sheet. Neutrinos are detected through Cherenkov radiation, emitted by charged secondary particles that are produced by neutrino interactions with nuclei in the ice or bedrock. Because of the large momentum transfer from the incoming neutrino, the directions of secondary particles are closely aligned with the incoming neutrino direction, enabling the identification of the neutrino's origin.

The two main detection channels are cascade and track events. Cascades are short-ranged particle showers, predominantly from interactions of electron neutrino (ν_e) and tau neutrino (ν_τ) with nuclei, as well as scatte[illegible] interactions of all three neutrino flavors [ν_e, muon neutrino (ν_μ), and ν_τ] on nuclei. Because the charged particles in cascade events travel only a few meters, these energy depositions appear almost point-like to IceCube's 125-m (horizontal) and 7- to 17-m (vertical) instrument spacing. This results in larger directional uncertainties than tracks. Tracks are elongated energy depositions (often several kilometers long), which arise predominantly from muons generated in cosmic-ray particle interactions in the atmosphere or muons produced by interactions of ν_μ with nuclei. The energy deposited by cascades is often contained within the instrumented volume (unlike tracks), which provides a more complete measure of the neutrino energy (*19*).

Searches for astrophysical neutrino sources are affected by an overwhelming background of muons and neutrinos produced by cosmic-ray interactions with Earth's atmosphere. Atmospheric muons dominate this background; IceCube records about 100 million muons for every observed astrophysical neutrino. Whereas muons from the Southern Hemisphere (above IceCube) can penetrate several kilometers deep into the ice, muons from the Northern Hemisphere (below IceCube) are absorbed during passage through Earth. Because of this shielding effect, and the superior angular resolution of tracks over cascades (≲1° compared with ≲10°, respectively; both above 10 TeV), searches for neutrino sources that use IceCube typically rely on track selections, making them most sensitive to astrophysical sources in the Northern sky (*20*).

The Galactic Center, as well as the bulk of the neutrino emission expected from the Galactic plane, is located in the Southern sky (Fig. 1, C and D). To overcome the muon background in the Southern sky, analyses of IceCube data often use events in which the neutrino interaction is observed within the detector (*21*, *22*). The selection of these events greatly reduces the background rate of cosmic-ray muons that enter the instrumented volume from the Southern sky. Unlike these atmospheric muons, atmospheric neutrinos (*23*) generally cannot be distinguished (by their interactions in the detector) from astrophysical neutrinos. Nevertheless, with increasing energy, an increasing fraction of the atmospheric neutrinos from the Southern sky (above IceCube) can be excluded by eliminating events with simultaneous muons that originate from the same cosmic-ray air-shower that produced the atmospheric neutrino (*24*, *25*). At the tera–electron volt energies relevant for searches of Galactic neutrino emission, the majority of these atmospheric neutrinos remain as a substantial background in searches for astrophysical neutrinos. This background is dominated by muon neutrinos, which are largely detected

*Corresponding author: analysis@icecube.wisc.edu; F. Halzen (francis.halzen@icecube.wisc.edu)
†IceCube Collaboration authors and affiliations are listed in the supplementary materials.

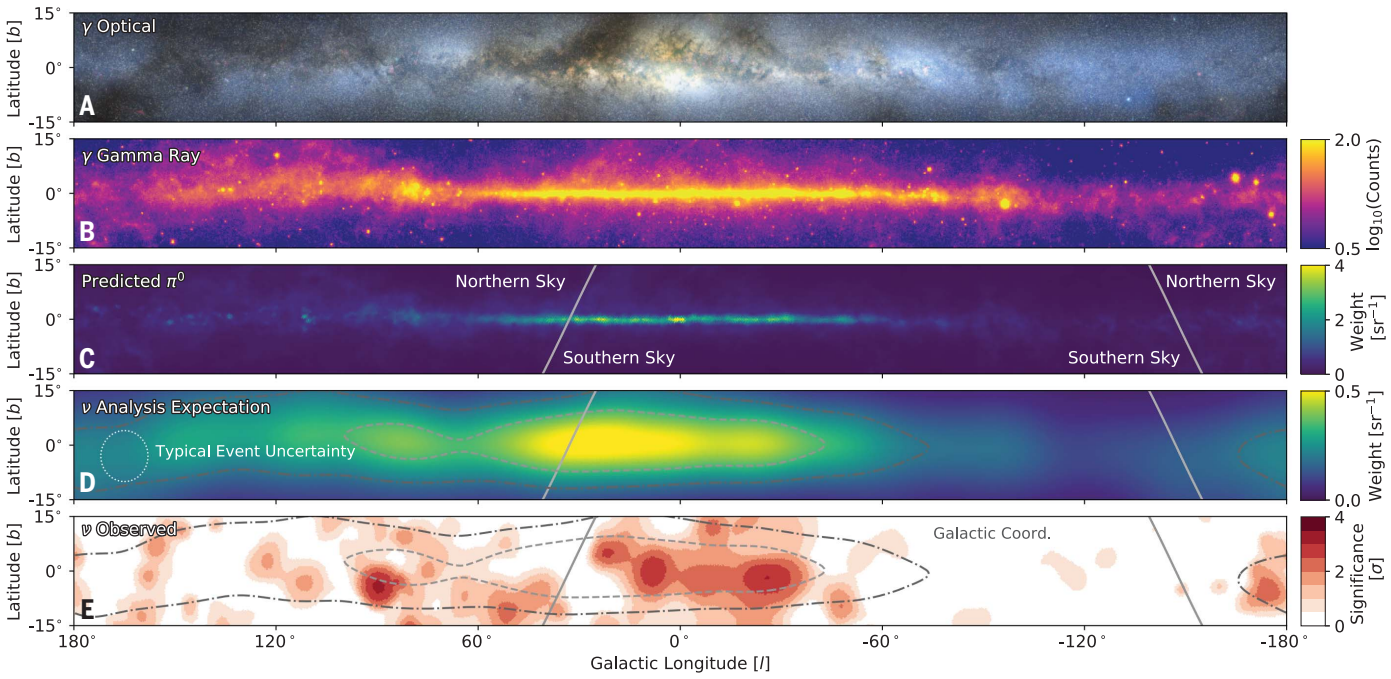

Fig. 1. The plane of the Milky Way Galaxy in photons and neutrinos. (A) to (E) are in Galactic coordinates, with the origin being at the Galactic Center, extending ±15° in latitude and ±180° in longitude. (**A**) Optical color image (*39*), which is partly obscured by clouds of gas and dust that absorb optical photons. [Credit: A. Mellinger, used with permission.] (**B**) The integrated flux in gamma rays from the Fermi Large Area Telescope (Fermi-LAT) 12-year survey (*40*) at energies greater than 1 GeV, obtained from the Fermi Science Support Center and processed with the Fermi-LAT ScienceTools. (**C**) The emission template calculated for the expected neutrino flux, derived from the π^0 template that matches the Fermi-LAT observations of the diffuse gamma-ray emission (*1*). (**D**) The emission template from (C), after including the detector sensitivity to cascade-like neutrino events and the angular uncertainty of a typical signal event (7°, indicated by the dotted white circle). Contours indicate the central regions that contain 20 and 50% of the predicted diffuse neutrino emission signal. (**E**) The pretrial significance of the IceCube neutrino observations, calculated from the all-sky scan for point-like sources by using the cascade neutrino event sample. Contours are the same as in (D). Gray lines in (C) to (E) indicate the northern-southern sky horizon at the IceCube detector.

as tracks in IceCube. The selection of cascade events instead of track events therefore reduces the contamination of atmospheric neutrinos—by about an order of magnitude at tera–electron volt energies—and permits the energy threshold of the analysis to be lowered to about 1 TeV.

In the Southern sky, the lower background, better energy resolution, and lower energy threshold of cascade events compensate for their inferior angular resolution, compared with those of tracks. This is particularly true for searches for emission from extended objects, such as the Galactic plane, for which the size of the emitting region is larger than (or similar to) the angular resolution. Compared with track-based searches, cascade-based analyses are more reliant on the signal purity and less on the angular resolution of individual events. We therefore expect analyses based on cascades to have substantially better sensitivity to extended neutrino emission in the tera–electron volt energy range from the Southern sky.

Application of deep learning to cascade events

To identify and reconstruct cascade events in IceCube, we used tools based on deep learning. These tools are designed to reject the overwhelming background from atmospheric muon events, then to identify the energies and directions of the neutrinos that generated the cascade events. IceCube observes events at a rate of about about 2.7 kHz (*18*), arising mostly from background events (atmospheric muons and atmospheric neutrinos) that outnumber signal events (astrophysical neutrinos) at a ratio of roughly 10^8:1. To search for neutrino sources, event selection was required to improve the signal purity by orders of magnitude.

Previously used event selections for cascade events (*22*, *26*, *27*) relied on high-level observables, such as the event location within the IceCube volume and total measured light levels, to reduce the initial data rate. In subsequent selection steps, more computing-intensive selection strategies were performed, such as the definition of veto regions within the detector, to further reject events identified as incoming muons. We adopted a different approach, using tools based on convolutional neural networks (CNNs) (*15*, *28*) to perform event selections. The high inference speed of the neural networks (milliseconds per event) allowed us to use a more complex filtering strategy at earlier stages of the event selection pipeline. This retains more low-energy astrophysical neutrino events (Fig. 2) and includes cascade events that are difficult to reconstruct and distinguish from background because of their location at the boundaries of the instrumented volume or in regions of the ice with degraded optical clarity (from higher concentrations of impurities in the ice).

After the selection of events, we refined event properties, such as the direction of the incoming neutrino and deposited energy, using the patterns of deposited light in the detector. The likelihood of the observed light pattern under a given event hypothesis was maximized to determine the event properties that best describe the data. For this purpose, we used a hybrid reconstruction method (*16*, *17*) that combines a maximum likelihood estimation with deep learning. In this approach, we used a neural network (NN) to parameterize the relationship between the event hypothesis and expected light yield in the detector. This smoothly approximates a (more computationally expensive) Monte Carlo simulation while avoiding the simplifications that limit other reconstruction methods (*19*, *29*). Starting with an event hypothesis, the NN models the photon

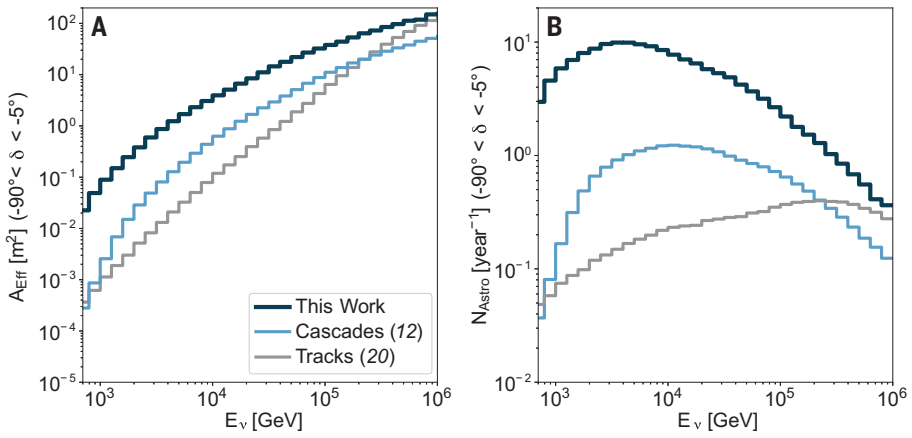

Fig. 2. Neutrino effective area and event selection comparison. (**A**) The all-flavor southern sky effective area (A_{Eff}) of the IceCube dataset, averaged over a solid angle in the declination (δ) range between −90° and −5° as a function of E_ν, the true neutrino energy. Results are shown for the deep learning event selection used in this work (dark blue), a previous cascade event selection (light blue) (*12*), and a previous track event selection (gray) (*20*) applied to the IceCube data. (**B**) The number of expected signal events (N_{Astro}) in the Southern sky per energy bin per year for each event selection, assuming an isotropic astrophysical flux (*22*). Calculations are based on equal contributions of each neutrino flavor at Earth because of neutrino oscillations.

yield at each DOM. Symmetries (such as rotation, translation, and time invariance of the neutrino interaction) and detector-specific domain knowledge are exploited by directly including them in the network architecture, which is analogous to how a Monte Carlo simulation would exploit this information. This differs from previous CNN-based methods used in neutrino telescopes (*15*), which inferred the event properties directly from the observed data. However, the observed IceCube data are already convolved with detector effects, making it difficult to exploit the underlying symmetries. Our hybrid method is intended to provide a more complete use of available information. A description of the hybrid method has been published previously (*16*), and we discuss its application to our dataset (*30*).

We found that this deep learning event selection retains more than 20 times as many events as that retained with the selection method used in the previous cascade-based Galactic plane analysis of IceCube data (Fig. 2) (*12*). It also provides improved angular resolution, by up to a factor of 2 at tera–electron volt energies (fig. S5) (*16*). The increased event rate is mostly due to the reduced energy threshold and the inclusion of events near the boundaries of the instrumented volume (fig. S3). We analyzed 10 years of IceCube data, collected between May 2011 and May 2021. A total of 59,592 events were selected over the entire sky in the energy range of 500 GeV to several peta–electron volts, compared with 1980 events from 7 years in the previous selection (*12*). We estimate that the remaining sample has an atmospheric muon contamination of about 6% (*30*), whereas the astrophysical neutrino contribution is estimated to about 7%, assuming the observed flux (*22*). The remaining 87% of the events are atmospheric neutrinos. These fractions are not used in the analysis directly; instead, we used the entire sample to derive a data-driven background estimate.

Searches for Galactic neutrino emission

We used this event selection to perform searches based on several neutrino emission hypotheses (*30*). For each hypothesis, we used a previously described maximum likelihood–based method (*31*), modified to account for signal contamination in the data-derived background model (*11*, *12*). These techniques, decided a priori and blind to the reconstructed event directions, infer the background from the data itself, avoiding the uncertainties introduced by background modeling. We calculated *P* values by comparing the experimental results with mock experiments performed on randomized experimental data. The backgrounds for these searches—consisting of atmospheric muons, atmospheric neutrinos, and the flux of extragalactic astrophysical neutrinos—are each largely isotropic. The rotation of Earth ensures that for a detector located at the South Pole, the detector sensitivity to neutrinos at different right ascensions is fairly uniform in each declination band. Therefore, we estimated backgrounds by scrambling the right ascension value of each event, preserving all detector-specific artifacts in the data. Any systematic differences between the modeling of signal hypotheses and the true signal could reduce the sensitivity of our search but would not invalidate the resulting *P* values.

The source hypothesis tests were defined a priori. They include tests for the diffuse emission expected from cosmic rays interacting with the interstellar medium in the Galactic plane, tests that use catalogs of known Galactic sources of tera–electron volt gamma rays, and a test for neutrino emission from the Fermi Bubbles (large areas of diffuse gamma-ray emission observed above and below the Galactic Center) (*32*). We also performed an all-sky point-like source search and a test for emission from a catalog of known giga–electron volt (mostly extragalactic) gamma-ray emitters (supplementary text). The results for each test (*30*) are summarized in Table 1.

Galactic plane neutrino searches

We tested three models of Galactic diffuse neutrino emission, extrapolated from the observations in gamma rays (Fig. 1B). These models are referred to as π^0, KRA_γ^5, and KRA_γ^{50} (*33*) and are each derived from the same underlying gamma-ray observations (*1*). The model predictions depend on the distribution and emission spectrum of cosmic-ray sources in the Galaxy, the properties of cosmic-ray diffusion in the interstellar medium, and the spatial distribution of target gas. Each neutrino emission model was converted to a spatial template, then convolved with the detector acceptance and the event's estimated angular uncertainty, to produce an event-specific spatial probability density function (shown for a typical event angular uncertainty of 7° in Fig. 1D).

The π^0 model assumes that the mega–electron volt–to–giga–electron volt π^0 component, inferred from the gamma-ray emission, follows a power law in photon energy (*E*) of $E^{-2.7}$ and can be extrapolated to tera–electron volt energies with the same spatial emission profile. The KRA_γ models include a variable spectrum in different spatial regions, use a harder (on average) neutrino spectrum than that of the π^0 model, and include a spectral cutoff at the highest energies (*33*). In this analysis, the KRA_γ models are tested with a template that uses a constant, model-averaged spectrum over the sky, roughly corresponding to an $E^{-2.5}$ power law, with either a 5 or 50 PeV cosmic-ray energy cutoff for the KRA_γ^5 and KRA_γ^{50} models, respectively. The KRA_γ models predict more concentrated neutrino emission from the Galactic Center region, whereas the π^0 model predicts events more evenly distributed along the Galactic plane. The corresponding neutrino spectrum predicted by each of these models has a cutoff at about 10 times lower energies.

We performed Galactic template searches with the same methods as those of previous Galactic diffuse emission searches (*11*, *12*). Because of the uncertainties in the expected distribution of sources, and their emission spectrum and cosmic-ray diffusion, we make no assumption about the absolute model normalization. Instead, the analyses include an unconstrained free parameter for the number of signal events (n_s) in the entire sky, which

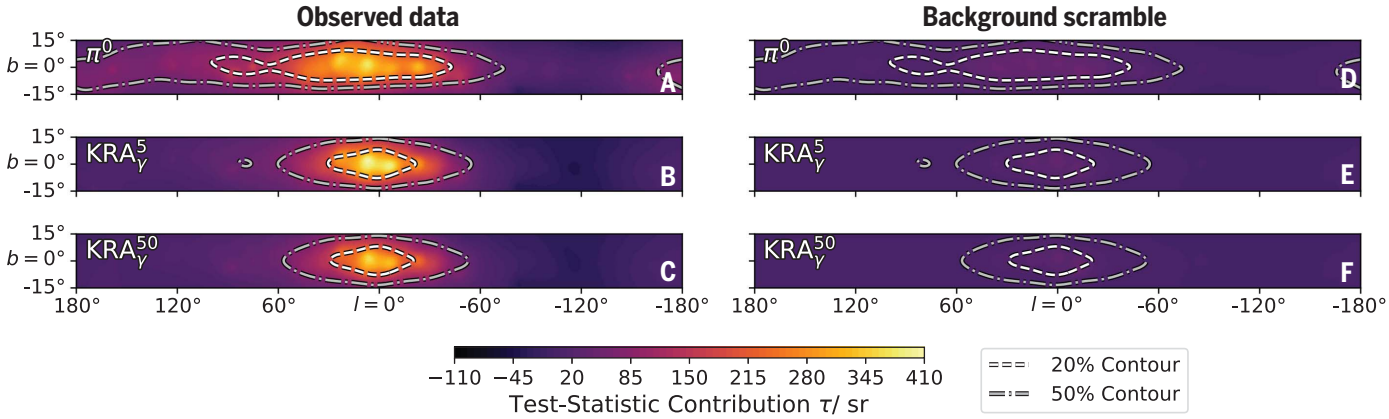

Fig. 3. Galactic plane test-statistic contributions. The contribution to the test-statistic τ is shown in galactic coordinates (longitude l and latitude b) for each of the three tested Galactic plane models. The overall test-statistic value was obtained through integration over the whole sky. (**A** to **C**) The contributions of each model for the observed data. (**D** to **F**) The contributions of each model for a single randomly selected mock experiment by using scrambled data. In (A) to (F), contours enclose 20% (white) and 50% (gray) of the predicted model flux; for the π^0 model, these are the same as in Fig. 1, D and E. The 50% contours contain about 1.64, 0.70, and 0.65 sr for the π^0, KRA_γ^5, and KRA_γ^{50} models, respectively.

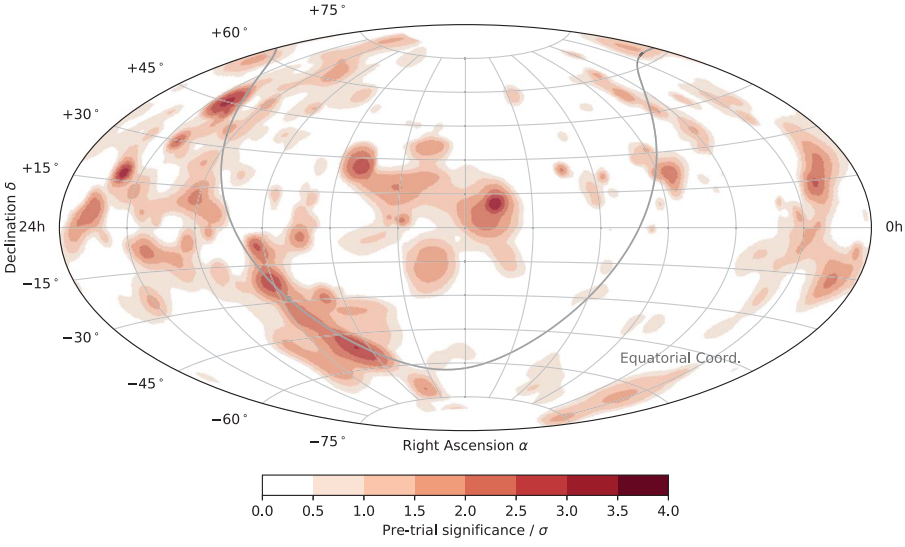

Fig. 4. All-sky point source search. A map of the best-fitting pretrial significance for the all-sky search, shown on an Aitoff projection of the celestial sphere, in equatorial coordinates (J2000 equinox). The Galactic plane is indicated with a grey curve, and the Galactic Center is indicated with a gray dot. Although some locations appear to have significant emission, the trial factor for the number of points searched means that these points are all individually statistically consistent with background fluctuations.

provides flux normalization, while keeping the spectrum fixed to the model. Results for each model are summarized in Table 1. We rejected the background-only hypothesis with significances of 4.71σ, 4.37σ, and 3.96σ for the π^0, KRA_γ^5, and KRA_γ^{50} models, respectively. Although these three hypotheses are correlated, we applied a conservative trial factor of 3 to the most significant of these values, leading to a trial-corrected P value equivalent to a significance of 4.48σ.

The best-fitting fluxes are also listed in Table 1. The flux normalization of the π^0 model is quoted at 100 TeV, assuming a single power law; however, the KRA_γ models have a more complex spectral prediction and are therefore quoted as multiples of the predicted model flux. These fluxes correspond to best-fitting values of 748, 276, and 211 signal events (n_s) in the IceCube dataset for the π^0, KRA_γ^5, and KRA_γ^{50} models, respectively. A visualization of the template results is shown in Fig. 3, A to C, in the form of a map of the per-steradian contribution to the results in the sky region near the Galactic Center for each of the Galactic plane models. Similar maps for a randomly selected mock experiment are also shown for comparison (Fig. 3, D to F).

An all-sky point source search was also performed (supplementary text), in which the sky was divided into a grid of equal solid-angle bins, spaced 0.45° apart, and each point was tested as a neutrino point source. The resulting significances are shown in Fig. 4. Some locations have excess emission over the background expectations, including some in spatial coincidence with known gamma-ray emitters, such as the Crab Nebula, 3C 454.3, and the Cygnus X region. However, after accounting for trial factors, no single point in the map is statistically significant (Table 1). This also implies that the emission that is present in the Galactic template analyses is not due to a single point source.

Searches using catalogs of Galactic sources

The total gamma-ray signal from the Galactic plane includes a contribution from several strong gamma-ray point sources (*1*). We therefore searched for correlated neutrino emission from three distinct catalogs of Galactic sources. Previous work had classified each source as a supernova remnant (SNR), pulsar wind nebula (PWN), or other unidentified (UNID) Galactic source, based on observations in tera–electron volt gamma rays (*34*, *35*). Under the assumption that multiple sources in each class emit neutrinos, stacking these sources in a single analysis provides higher sensitivity compared

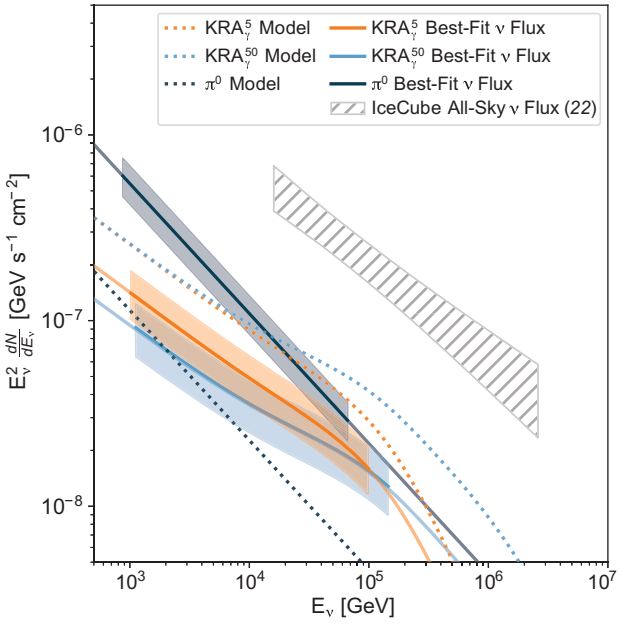

Fig. 5. Energy spectra for each of the Galactic plane models. Energy-scaled, sky-integrated, per-flavor neutrino flux is shown as a function of neutrino energy (E_ν) for each of the Galactic plane models. Dotted lines are the predicted values for the π^0 (dark blue), KRA$_\gamma^5$ (orange), and KRA$_\gamma^{50}$ (light blue) models. Solid lines are our best-fitting flux normalizations from the IceCube data. Shaded regions indicate the 1σ uncertainties; they extend over the energy range that contributes to 90% of the significance. These results are based on the all-sky (4π sr) template and are presented as an all-sky flux. For comparison, the gray hatching shows the IceCube total neutrino flux (*22*), scaled to an all-sky flux by multiplying by 4π, with its 1σ uncertainty.

Table 1. Summarized results of the neutrino emission searches. The flux sensitivity and best-fitting flux normalization (Φ) are given in units of model flux (MF) for the KRA$_\gamma$ templates and for the π^0 analyses as $E^2 \frac{dN}{dE}$ at 100 TeV, in units of 10^{-12} TeV cm^{-2} s^{-1} (where $\frac{dN}{dE}$ is the differential number of neutrinos per flavor, *N*, and neutrino energy, *E*). *P* values and significances are calculated with respect to the background-only hypothesis. Pretrial *P* values for each individual result are listed for the three diffuse Galactic plane analyses and three stacking analyses, and posttrial *P* values are given for the other analyses (supplementary text). Because of the spatial overlap of the stacking catalogs with the diffuse Galactic plane templates, strong correlations between these searches are expected. More detailed results for each search are provided in tables S1 to S5.

	Flux sensitivity Φ	*P* value	Best-fitting flux Φ
Diffuse Galactic plane analysis			
π^0	5.98	1.26×10^{-6} (4.71σ)	$21.8^{+5.3}_{-4.9}$
KRA$_\gamma^5$	0.16 × MF	6.13×10^{-6} (4.37σ)	$0.55^{+0.18}_{-0.15}$ × MF
KRA$_\gamma^{50}$	0.11 × MF	3.72×10^{-5} (3.96σ)	$0.37^{+0.13}_{-0.11}$ × MF
Catalog stacking analysis			
SNR		5.90×10^{-4} (3.24σ)*	
PWN		5.93×10^{-4} (3.24σ)*	
UNID		3.39×10^{-4} (3.40σ)*	
Other analyses			
Fermi bubbles		0.06 (1.52σ)	
Source list		0.22 (0.77σ)	
Hotspot (north)		0.28 (0.58σ)	
Hotspot (south)		0.46 (0.10σ)	

*Significance values that are consistent with the diffuse Galactic plane template search results.

with individual source searches, because the neutrino fluxes add together, whereas random background adds incoherently (*36*). The objects in each catalog were selected according to the observed gamma-ray emission above 100 GeV and the detector sensitivity, following previously described methods (*20*). We chose the 12 sources from each category with the strongest expected neutrino flux and weighted them under the hypothesis that each contributes equally to the flux (supplementary text). The total number of signal events and the spectral index are left as free parameters for each catalog search. The resulting *P* value for each catalog search is shown in Table 1. Each result rejects the background-only hypothesis at the 3σ level or above. However, we do not interpret these neutrino event excesses as a detection because the objects in these Galactic source catalogs overlap spatially with regions that predict the largest neutrino fluxes in the Galactic plane diffuse emission searches.

Implications of Galactic neutrinos

The neutrino flux we observed from the Galactic plane could arise from several different emission mechanisms. The predicted energy spectra integrated over the entire sky is shown in Fig. 5 for each of the Galactic plane models and their best-fitting flux normalization. Model-to-model flux comparisons depend on the regions of the sky considered. The KRA$_\gamma$ best-fitting flux normalizations are lower than predicted, which could indicate a spectral cutoff that is inconsistent with the 5 and 50 PeV values assumed. The simpler extrapolation of the π^0 model from giga–electron volt energies to 100 TeV predicts a neutrino flux that is a factor of ~5 below our best-fitting flux. However, the best-fitting flux for the π^0 model appear to be consistent with recent observations of 100-TeV gamma rays by the Tibet Air Shower Array (fig. S8) (*37*). The π^0 model mismatch could arise from propagation or spectral differences for cosmic rays in the Galactic Center region, or from contributions from unresolved neutrino sources.

We used model injection tests to quantify the ambiguity between different source hypotheses. In these tests, the best-fitting neutrino signal from one source search was simulated, then the expected results in all other analyses were examined. Injecting a signal from the π^0 model analysis, with a flux normalization equal to the best-fitting value from the observations, produces a median significance that is consistent with the best-fitting values for all other tested hypotheses (within the expected statistical fluctuations). This includes the 3σ excess observed in Galactic source catalog searches. Individually injecting the best-fitting flux of any one of the tested Galactic source catalogs, at the flux level observed, did not recover the observed π^0 or KRA$_\gamma$ model results. However, the angular resolution of the sample and the small number of equally weighted sources included in these catalogs does not constrain emissions from these broad source populations. It is plausible that many independently contributing sources from the Galactic plane could show a similar result to diffuse emission from interactions in the interstellar medium. These tests favor a neutrino signal from Galactic plane diffuse emission, but we do not have sufficient statistical power to differentiate between the tested emission models or identify embedded point sources.

The neutrinos observed from the Galactic plane contribute to the all-sky astrophysical diffuse flux previously observed by IceCube (Fig. 5) (*21*, *22*, *38*). The fluxes we infer for each of the Galactic template models contribute

~6 to 13% of the astrophysical flux at 30 TeV. These comparisons are complicated because of different spectral assumptions and tested energy ranges used in each analysis. Additionally, the observed Galactic flux is integrated over the entire sky, so local emission along the central region of the Galactic Plane contributes a higher fraction to the total flux.

The observed excess of neutrinos from the Galactic plane provides strong evidence that the Milky Way is a source of high-energy neutrinos. This evidence is consistent with the expected interactions of cosmic rays within the Galaxy, as established with gamma-ray measurements. It complements IceCube's measurements of the diffuse extragalactic flux to provide a more complete picture of the neutrino sky.

REFERENCES AND NOTES

1. M. Ackermann *et al*., *Astrophys. J.* **750**, 3 (2012).
2. F. W. Stecker, *Astrophys. J.* **228**, 919 (1979).
3. V. Berezinsky, T. Gaisser, F. Halzen, T. Stanev, *Astropart. Phys.* **1**, 281–287 (1993).
4. G. Ingelman, M. Thunman, arXiv:hep-ph/9604286 (1996).
5. C. Evoli, D. Grasso, L. Maccione, *J. Cosmol. Astropart. Phys.* **2007**, 003 (2007).
6. M. Ackermann *et al*., *Science* **339**, 807–811 (2013).
7. D. Guetta, E. Amato, *Astropart. Phys.* **19**, 403–407 (2003).
8. W. Bednarek, *Astron. Astrophys.* **407**, 1–6 (2003).
9. M. C. Gonzalez-Garcia, F. Halzen, S. Mohapatra, *Astropart. Phys.* **31**, 437–444 (2009).
10. F. Halzen, A. Kheirandish, V. Niro, *Astropart. Phys.* **86**, 46–56 (2017).
11. M. G. Aartsen *et al*., *Astrophys. J.* **849**, 67 (2017).
12. M. G. Aartsen *et al*., *Astrophys. J.* **886**, 12 (2019).
13. A. Albert *et al*., *Astrophys. J. Lett.* **868**, L20 (2018).
14. A. Albert *et al*., *Phys. Rev. D* **96**, 062001 (2017).
15. R. Abbasi *et al*., *J. Instrum.* **16**, P07041 (2021).
16. The IceCube Collaboration, Combining maximum-likelihood with deep learning for event reconstruction in IceCube, presented at 2021 ICRC The Astroparticle Physics Conference, 12 to 23 Junly 2021, Berlin, Germany, 10.22323/1.395.1065 (2021).
17. M. Huennefeld, icecube/event-generator: Version 1.0.2. Zenodo (2022); https://doi.org/10.5281/zenodo.7412035.
18. M. Aartsen *et al*., *J. Instrum.* **12**, P03012 (2017).
19. M. Aartsen *et al*., *J. Instrum.* **9**, P03009 (2014).
20. M. G. Aartsen *et al*., *Phys. Rev. Lett.* **124**, 051103 (2020).
21. R. Abbasi *et al*., *Phys. Rev. D* **104**, 022002 (2021).
22. M. G. Aartsen *et al*., *Phys. Rev. Lett.* **125**, 121104 (2020).
23. T. K. Gaisser, M. Honda, *Annu. Rev. Nucl. Part. Sci.* **52**, 153–199 (2002).
24. S. Schönert, T. K. Gaisser, E. Resconi, O. Schulz, *Phys. Rev. D Part. Fields Gravit. Cosmol.* **79**, 043009 (2009).
25. T. K. Gaisser, K. Jero, A. Karle, J. van Santen, *Phys. Rev. D Part. Fields Gravit. Cosmol.* **90**, 023009 (2014).
26. M. G. Aartsen *et al*., *Phys. Rev. D Part. Fields Gravit. Cosmol.* **91**, 022001 (2015).
27. IceCube Collaboration, *Science* **342**, 1242856 (2013).
28. Y. LeCun *et al*., *Advances in Neural Information Processing Systems 2* (Morgan-Kaufmann, 1990), pp. 396–404.
29. R. Abbasi *et al*., *J. Instrum.* **16**, P08034 (2021).
30. Materials and methods are available as supplementary materials.
31. J. Braun *et al*., *Astropart. Phys.* **29**, 299–305 (2008).
32. M. Su, T. R. Slatyer, D. P. Finkbeiner, *Astrophys. J.* **724**, 1044–1082 (2010).
33. D. Gaggero, D. Grasso, A. Marinelli, A. Urbano, M. Valli, *Astrophys. J. Lett.* **815**, L25 (2015).
34. S. Wakely, D. Horan, TeVCat, http://tevcat2.uchicago.edu (2022).
35. A. Voruganti, C. Deil, A. Donath, J. King in *6th International Symposium on High Energy Gamma-Ray Astronomy* (AIP Conference Proceedings, 2017) 1792, p. 070005; http://gamma-sky.net/.
36. R. Abbasi *et al*., *Astrophys. J.* **732**, 18 (2011).
37. M. Amenomori *et al*., *Phys. Rev. Lett.* **126**, 141101 (2021).
38. R. Abbasi *et al*., *Astrophys. J.* **928**, 50 (2022).
39. A. Mellinger, *Publ. Astron. Soc. Pac.* **121**, 1180–1187 (2009).
40. Fermi's 12-year view of the gamma-ray sky, NASA Goddard Space Flight Center (2022); https://svs.gsfc.nasa.gov/14090.

ACKNOWLEDGMENTS

The IceCube Collaboration thanks D. Gaggero, D. Grasso, A. Marinelli, A. Urbano, and M. Valli for providing the templates for the KRA-γ models and for fruitful discussions. **Funding:** The authors gratefully acknowledge support from the following agencies and institutions. USA: US National Science Foundation–Office of Polar Programs, US National Science Foundation–Physics Division, US National Science Foundation–EPSCoR, Wisconsin Alumni Research Foundation, Center for High Throughput Computing (CHTC) at the University of Wisconsin–Madison, Open Science Grid (OSG), Extreme Science and Engineering Discovery Environment (XSEDE), Frontera computing project at the Texas Advanced Computing Center, US Department of Energy–National Energy Research Scientific Computing Center, Particle Astrophysics Research Computing center at the University of Maryland, Institute for Cyber-Enabled Research at Michigan State University, and Astroparticle physics computational facility at Marquette University. Belgium: Funds for Scientific Research (FRS-FNRS and FWO), FWO Odysseus and Big Science programmes, and Belgian Federal Science Policy Office (Belspo). Germany: Bundesministerium für Bildung und Forschung (BMBF), Deutsche Forschungsgemeinschaft (DFG), Helmholtz Alliance for Astroparticle Physics (HAP), Initiative and Networking Fund of the Helmholtz Association, Deutsches Elektronen Synchrotron (DESY), and High Performance Computing cluster of the RWTH Aachen. Sweden: Swedish Research Council, Swedish Polar Research Secretariat, Swedish National Infrastructure for Computing (SNIC), and Knut and Alice Wallenberg Foundation. Australia: Australian Research Council. Canada: Natural Sciences and Engineering Research Council of Canada, Calcul Québec, Compute Ontario, Canada Foundation for Innovation, WestGrid, and Compute Canada. Denmark: Villum Fonden and Carlsberg Foundation. New Zealand: Marsden Fund. Japan: Japan Society for Promotion of Science (JSPS) and Institute for Global Prominent Research (IGPR) of Chiba University. Korea: National Research Foundation of Korea (NRF). Switzerland: Swiss National Science Foundation (SNSF). United Kingdom: Department of Physics, University of Oxford. **Author contributions:** Major contributions to this manuscript were made by M. Hünnefeld and S. Sclafani. The IceCube Collaboration designed, constructed, and now operates the IceCube Neutrino Observatory. Data processing and calibration, Monte Carlo simulations of the detector and of theoretical models, and data analyses were performed by a large number of collaboration members, who also discussed and approved the scientific results. The manuscript was reviewed by the entire collaboration before publication, and all authors approved the final version. Contributions are in the areas of (a) Conceptualization, Formal Analysis, and Methodology; (b) Data Curation and Resources; (c) Funding Acquisition and Project Administration; (d) Investigation; (e) Software; (f) Supervision; (g) Validation; (h) Writing – original draft and visualization; and (i) Writing – review and editing. M. Ackermann (b, c, d), J. Adams (d, e, g), M. Ahlers (c, d, i), M. Ahrens (d), J. M. Alameddine (d), A. A. Alves Jr. (e), N. M. Amin (d), K. Andeen (b, c, d), T. Anderson (d), G. Anton (c, d), C. Argüelles (b, d), Y. Ashida (d), S. Athanasiadou (d), S. Axani (e), X. Bai (a, c, d), A. Balagopal V. (d), V. Basu (d), R. Bay (b, d), J. J. Beatty (d), K.-H. Becker (d), J. Becker Tjus (c, d), J. Beise (d), C. Bellenghi (b, e), S. Benda (d), D. Berley (c), E. Bernardini (c, d), D. Bindig (d), E. Blaufuss (a, b, c, d, e, g, h, i), S. Blot (c, d), F. Bontempo (d), J. Borowka (g, i), S. Böser (c, d), O. Botner (a, b, c, d, i), J. Böttcher (b, e, g, i), E. Bourbeau (d), F. Bradascio (d), J. Braun (b, d, e), B. Brinson (d), J. Brostean-Kaiser (d), R. T. Burley (d), R. S. Busse (d), M. A. Campana (d, e), E. G. Carnie-Bronca (d), C. Chen (d), D. Chirkin (b, d, e), B. A. Clark (d), L. Classen (d), A. Coleman (b, d, e), G. H. Collin (e), J. M. Conrad (d), P. Coppin (d), P. Correa (d), D. F. Cowen (c, d), C. Dappen (b, g, i), P. Dave (d), C. De Clercq (c, d), J. J. DeLaunay (b, g, i), D. Delgado López (d), H. Dembinski (b, d, e), K. Deoskar (d), A. Desai (d), P. Desiati (b, c, d, e), K. D. de Vries (d), G. de Wasseige (d), T. DeYoung (b, c, d), A. Diaz (e), J. C. Díaz-Vélez (b, d, e), M. Dittmer (d), H. Dujmovic (d), M. Dunkman (d), M. A. DuVernois (b, d), T. Ehrhardt (d), P. Eller (b, e), R. Engel (f), H. Erpenbeck (b, g, i), J. Evans (b, d), P. A. Evenson (b, d), K. L. Fan (b, d), A. Fedynitch (d), N. Feigl (d), S. Fiedlschuster (d), A. T. Fienberg (d), C. Finley (a, c, d, g, h), L. Fischer (d), D. Fox (d), A. Franckowiak (c, d), E. Friedman (b, d, e), A. Fritz (d), P. Fürst (a, b, e, g, i), T. K. Gaisser (a, b, c, d), J. Gallagher (b, d), E. Ganster (b, e, g, i), A. Garcia (d), S. Garrappa (d), L. Gerhardt (b, d), A. Ghadimi (b), C. Glaser (d), T. Glauch (b, e), T. Glüsenkamp (d), N. Goehlke (d), A. Goldschmidt (a, c, d), J. G. Gonzalez (b, c, d, e), S. Goswami (b), D. Grant (c, d), T. Grégoire (d), C. Günther (g, i), P. Gutjahr (d), C. Haack (b, d, g), A. Hallgren (a, b, c, d), R. Halliday (b, d), L. Halve (g, i), F. Halzen (a, b, c, d, h, i), M. Ha Minh (e), K. Hanson (b, c, d, e), J. Hardin (b, d, e), A. A. Harnisch (d, e), A. Haungs (c, f), K. Helbing (d), F. Henningsen (e), S. Hickford (d), J. Hignight (d, e), C. Hill (b), G. C. Hill (a, b, c, d), K. D. Hoffman (b, c, d), K. Hoshina (b, d, e), W. Hou (d), F. Huang (d), M. Huber (b, e), T. Huber (d), K. Hultqvist (c, d), M. Hünnefeld (a, d, e, h, i), R. Hussain (b, d, e), K. Hymon (d), S. In (d), A. Ishihara (b, c, d, e), M. Jansson (d, e), G. S. Japaridze (d), M. Jeong (d), D. Kang (d), W. Kang (d), X. Kang (d, e), A. Kappes (c, d), D. Kappesser (d), L. Kardum (d), T. Karg (b, c, d), M. Karl (b, e), A. Karle (a, b, c, d, i), U. Katz (c, d), M. Kauer (b, d, e), M. Kellermann (g, i), J. L. Kelley (b, c, d, e), A. Kheirandish (d, i), K. Kin (b), S. R. Klein (a, c, d), A. Kochocki (d), R. Koirala (d), H. Kolanoski (c, d), T. Kontrimas (b, e), L. Köpke (c, d), C. Kopper (b, c, d, e, g, i), D. J. Koskinen (c, d), P. Koundal (d), M. Kovacevich (d, e), M. Kowalski (b, c, d), T. Kozynets (d), E. Krupczak (d), E. Kun (d), N. Kurahashi (a, b, c, d, e, f, g, h, i), N. Lad (d), C. Lagunas Gualda (d), J. L. Lanfranchi (d), M. J. Larson (b, c, d, e), F. Lauber (d), J. P. Lazar (b, d), K. Leonard (b, d, e), A. Leszczyńska (b, c, d, e), Y. Li (d), M. Lincetto (b, d), Q. R. Liu (b, d, e), M. Liubarska (d), E. Lohfink (d), C. J. Lozano Mariscal (d), L. Lu (b, d, e), F. Lucarelli (a, d, e), A. Ludwig (d), W. Luszczak (b, d, e), Y. Lyu (d), W. Y. Ma (d), J. Madsen (c, d), K. B. M. Mahn (d), Y. Makino (b, d), S. Mancina (b, d, e), I. Martinez-Soler (d), R. Maruyama (c, d), S. McCarthy (d), T. McElroy (d), F. McNally (d), J. V. Mead (d), K. Meagher (b, d, e), S. Mechbal (d), A. Medina (d, e), M. Meier (e), S. Meighen-Berger (e), Y. Merckx (d), J. Micallef (d), T. Montaruli (a, b, d, e), R. W. Moore (d), R. Morse (a, b, c, d), M. Moulai (b, d, e), T. Mukherjee (d), R. Naab (d), R. Nagai (b), R. Nahnhauer (b, d), U. Naumann (d), J. Necker (d), H. Niederhausen (b, d, g, i), M. U. Nisa (d), S. C. Nowicki (d), A. Obertacke Pollmann (d), M. Oehler (d), B. Oeyen (d), A. Olivas (b, c, d, e), E. O'Sullivan (c, d), H. Pandya (d), D. V. Pankova (d), N. Park (a, b, c, i), E. N. Paudel (d), L. Paul (b, d), C. Pérez de los Heros (a, b, c, d), L. Peters (b, g, i), J. Peterson (d), S. Philippen (b, e, g, i), S. Pieper (d), A. Pizzuto (b, d, e), M. Plum (b, e), Y. Popovych (d), A. Porcelli (d), M. Prado Rodriguez (b, d, e), B. Pries (d), J. Rack-Helleis (d), K. Rawlins (b, c, d, e), I. C. Rea (e), Z. Rechav (d), A. Rehman (d), P. Reichherzer (d), R. Reimann (b, e, g, i), E. Resconi (a, b, f, i), S. Reusch (d), W. Rhode (b, c, d, f), M. Richman (a, b, d, e, g), B. Riedel (b, c, d, e), E. J. Roberts (d), G. Roellinghoff (d), M. Rongen (d), C. Rott (b, c, d), T. Ruhe (b, c, d), D. Ryckbosch (c, d), D. Rysewyk Cantu (d), I. Safa (b, d, e), J. Saffer (d), D. Salazar-Gallegos (d), P. Sampathkumar (d), S. E. Sanchez Herrera (d), A. Sandrock (d), M. Santander (b, c, i), S. Sarkar (d), K. Satalecka (d), M. Schaufel (g, i), H. Schieler (d), S. Schindler (d), T. Schmidt (b, d, e), A. Schneider (b, d, e), J. Schneider (d), F. G. Schröder (b, c, d), L. Schumacher (a, b, e), G. Schwefer (a, b, d, e, g, i), S. Sclafani (a, b, d, e, h, i), D. Seckel (a, b, c, d), A. Sharma (d), S. Shefali (d), N. Shimizu (b), M. Silva (b, d, e), B. Skrzypek (d), R. Snihur (b, d, e), J. Soedingrekso (d), D. Soldin (b, c, d, e), C. Spannfellner (e), G. M. Spiczak (d), C. Spiering (b, c, d), M. Stamatikos (d), T. Stanev (a, d), R. Stein (d), J. Stettner (b, e, g, i), B. Stokstad (a, c, d), T. Stürwald (d), T. Stuttard (c, d), G. W. Sullivan (b, c, d), I. Taboada (c, d, i), J. Thwaites (d), S. Tilav (a, b, c, d, e, g), F. Tischbein (g, i), K. Tollefson (c, d), C. Tönnis (d), D. Tosi (b, d, e), A. Trettin (d), M. Tselengidou (d), C. F. Tung (d), A. Turcati (b, e), R. Turcotte (d), C. F. Turley (d), J. P. Twagirayezu (d), B. Ty (d), M. A. Unland Elorrieta (d), N. Valtonen-Mattila (b, d), J. Vandenbroucke (b, c, d, e, h, i), N. van Eijndhoven (c, d), D. Vannerom (e), J. van Santen (b, c, d, e), J. Veitch-Michaelis (b, d), S. Verpoest (d), C. Walck (d), W. Wang (d), C. Weaver (d, e), P. Weigel (e), A. Weindl (d), M. J. Weiss (d), J. Weldert (d), C. Wendt (b, c, d, e), J. Werthebach (d), M. Weyrauch (d), N. Whitehorn (c, d, e, i), C. H. Wiebusch (a, c, d, f, g, i), N. Willey (d), D. R. Williams (c, d, e, i), M. Wolf (b, d, e), G. Wrede (d), J. P. Yanez (d, e), S. Yu (b, d, e, g, i), S. Yoshida (b, c, d), E. Yildizci (d), and T. Yuan (b, c, d, e). **Competing interests:** There are no competing interests to declare. **Data and materials availability:** The data and analysis software used in this paper are available from the IceCube data archive: https://icecube.wisc.edu/science/data/neutrino-emission-galactic-plane. The event selection code is archived at Zenodo (*17*).

SUPPLEMENTARY MATERIALS

science.org/doi/10.1126/science.adc9818
Materials and Methods
Supplementary Text
Figs. S1 to S12
Tables S1 to S5
IceCube Collaboration Authors
References (*41*–*62*)

Submitted 12 May 2022; accepted 4 May 2023
10.1126/science.adc9818

Science
AAAS

Observation of high-energy neutrinos from the Galactic plane

IceCube Collaboration*, R. Abbasi, M. Ackermann, J. Adams, J. A. Aguilar, M. Ahlers, M. Ahrens, J. M. Alameddine, A. A. Alves, Jr., N. M. Amin, K. Andeen, T. Anderson, G. Anton, C. Argelles, Y. Ashida, S. Athanasiadou, S. Axani, X. Bai, A. Balagopal V., S. W. Barwick, V. Basu, S. Baur, R. Bay, J. J. Beatty, K.-H. Becker, J. Becker Tjus, J. Beise, C. Bellenghi, S. Benda, S. BenZvi, D. Berley, E. Bernardini, D. Z. Besson, G. Binder, D. Bindig, E. Blaufuss, S. Blot, M. Boddenberg, F. Bontempo, J. Y. Book, J. Borowka, S. Bser, O. Botner, J. Bttcher, E. Bourbeau, F. Bradascio, J. Braun, B. Brinson, S. Bron, J. Brostean-Kaiser, R. T. Burley, R. S. Busse, M. A. Campana, E. G. Carnie-Bronca, C. Chen, Z. Chen, D. Chirkin, K. Choi, B. A. Clark, K. Clark, L. Classen, A. Coleman, G. H. Collin, A. Connolly, J. M. Conrad, P. Coppin, P. Correa, D. F. Cowen, R. Cross, C. Dappen, P. Dave, C. De Clercq, J. J. DeLaunay, D. Delgado Lpez, H. Dembinski, K. Deoskar, A. Desai, P. Desiati, K. D. de Vries, G. de Wasseige, T. DeYoung, A. Diaz, J. C. Daz-Vlez, M. Dittmer, H. Dujmovic, M. Dunkman, M. A. DuVernois, T. Ehrhardt, P. Eller, R. Engel, H. Erpenbeck, J. Evans, P. A. Evenson, K. L. Fan, A. R. Fazely, A. Fedynitch, N. Feigl, S. Fiedlschuster, A. T. Fienberg, C. Finley, L. Fischer, D. Fox, A. Franckowiak, E. Friedman, A. Fritz, P. Frst, T. K. Gaisser, J. Gallagher, E. Ganster, A. Garcia, S. Garrappa, L. Gerhardt, A. Ghadimi, C. Glaser, T. Glauch, T. Glsenkamp, N. Goehlke, A. Goldschmidt, J. G. Gonzalez, S. Goswami, D. Grant, T. Grgoire, S. Griswold, C. Gnther, P. Gutjahr, C. Haack, A. Hallgren, R. Halliday, L. Halve, F. Halzen, M. Ha Minh, K. Hanson, J. Hardin, A. A. Harnisch, A. Haungs, K. Helbing, F. Henningsen, E. C. Hettinger, S. Hickford, J. Hignight, C. Hill, G. C. Hill, K. D. Hoffman, K. Hoshina, W. Hou, F. Huang, M. Huber, T. Huber, K. Hultqvist, M. Hnnefeld, R. Hussain, K. Hymon, S. In, N. Iovine, A. Ishihara, M. Jansson, G. S. Japaridze, M. Jeong, M. Jin, B. J. P. Jones, D. Kang, W. Kang, X. Kang, A. Kappes, D. Kappesser, L. Kardum, T. Karg, M. Karl, A. Karle, U. Katz, M. Kauer, M. Kellermann, J. L. Kelley, A. Kheirandish, K. Kin, J. Kiryluk, S. R. Klein, A. Kochocki, R. Koirala, H. Kolanoski, T. Kontrimas, L. Kpke, C. Kopper, S. Kopper, D. J. Koskinen, P. Koundal, M. Kovacevich, M. Kowalski, T. Kozynets, E. Krupczak, E. Kun, N. Kurahashi, N. Lad, C. Lagunas Gualda, J. L. Lanfranchi, M. J. Larson, F. Lauber, J. P. Lazar, J. W. Lee, K. Leonard, A. Leszczyska, Y. Li, M. Lincetto, Q. R. Liu, M. Liubarska, E. Lohfink, C. J. Lozano Mariscal, L. Lu, F. Lucarelli, A. Ludwig, W. Luszczak, Y. Lyu, W. Y. Ma, J. Madsen, K. B. M. Mahn, Y. Makino, S. Mancina, I. C. Mari, I. Martinez-Soler, R. Maruyama, S. McCarthy, T. McElroy, F. McNally, J. V. Mead, K. Meagher, S. Mechbal, A. Medina, M. Meier, S. Meighen-Berger, Y. Merckx, J. Micallef, D. Mockler, T. Montaruli, R. W. Moore, K. Morik, R. Morse, M. Moulai, T. Mukherjee, R. Naab, R. Nagai, R. Nahnhauer, U. Naumann, J. Necker, L. V. Nguyen, H. Niederhausen, M. U. Nisa, S. C. Nowicki, D. Nygren, A. Obertacke Pollmann, M. Oehler, B. Oeyen, A. Olivas, E. O'Sullivan, H. Pandya, D. V. Pankova, N. Park, G. K. Parker, E. N. Paudel, L. Paul, C. Prez de los Heros, L. Peters, J. Peterson, S. Philippen, S. Pieper, A. Pizzuto, M. Plum, Y. Popovych, A. Porcelli, M. Prado Rodriguez, B. Pries, G. T. Przybylski, C. Raab, J. Rack-Helleis, A. Raissi, M. Rameez, K. Rawlins, I. C. Rea, Z. Rechav, A. Rehman, P. Reichherzer, R. Reimann, G. Renzi, E. Resconi, S. Reusch, W. Rhode, M. Richman, B. Riedel, E. J. Roberts, S. Robertson, G. Roellinghoff, M. Rongen, C. Rott, T. Ruhe, D. Ryckbosch, D. Rysewyk Cantu, I. Safa, J. Saffer, D. Salazar-Gallegos, P. Sampathkumar, S. E. Sanchez Herrera, A. Sandrock, M. Santander, S. Sarkar, S. Sarkar, K. Satalecka, M. Schaufel, H. Schieler, S. Schindler, T. Schmidt, A. Schneider, J. Schneider, F. G. Schrder, L. Schumacher, G. Schwefer, S. Sclafani, D. Seckel, S. Seunarine, A. Sharma, S. Shefali, N. Shimizu, M. Silva, B. Skrzypek, B. Smithers, R. Snihur, J. Soedingrekso, A. Sogaard, D. Soldin, C. Spannfellner, G. M. Spiczak, C. Spiering, M. Stamatikos, T. Stanev, R. Stein, J. Stettner, T. Stezelberger, B. Stokstad, T. Strwald, T. Stuttard, G. W. Sullivan, I. Taboada, S. Ter-Antonyan, J. Thwaites, S. Tilav, F. Tischbein, K. Tollefson, C. Tnnis, S. Toscano, D. Tosi, A. Trettin, M. Tselengidou, C. F. Tung, A. Turcati, R. Turcotte, C. F. Turley, J. P. Twagirayezu, B. Ty, M. A. Unland Elorrieta, N. Valtonen-Mattila, J. Vandenbroucke, N. van Eijndhoven, D. Vannerom, J. van Santen, J. Veitch-Michaelis, S. Verpoest, C. Walck, W. Wang, T. B. Watson, C. Weaver, P. Weigel, A. Weindl, M. J. Weiss, J. Weldert, C. Wendt, J. Werthebach, M. Weyrauch, N. Whitehorn, C. H. Wiebusch, N. Willey, D. R. Williams, M. Wolf, G. Wrede, J. Wulff, X. W. Xu, J. P. Yanez, E. Yildizci, S. Yoshida, S. Yu, T. Yuan, Z. Zhang, and P. Zhelnin

Science, **380** (6652), .
DOI: 10.1126/science.adc9818

Editor's summary

Observations of high-energy astrophysical neutrinos have shown that they mostly originate from extragalactic sources such as active galaxies. However, gamma ray observations show bright emission from within the Milky Way galaxy,

and astrophysical gamma rays and neutrinos are expected to be produced by the same physical processes. The IceCube Collaboration searched for neutrino emission from within the Milky Way (see the Perspective by Fusco) and found evidence of extra neutrinos emitted along the plane of the Galaxy, which is consistent with the distribution of gamma-ray emission. These results imply that high-energy neutrinos can be generated by nearby sources within the Milky Way. —Keith T. Smith